Supplementary information

Second harmonic generation polarization microscopy as a tool for protein structure analysis

Junichi Kaneshiro[1], Yasushi Okada[2,3], Tomohiro Shima[2,4], Mika Tsujii[5], Katsumi Imada[5], Taro Ichimura[1]*, Tomonobu M. Watanabe[1]*

[1]Laboratory for Comprehensive Bioimaging, RIKEN Center for Biosystems Dynamics Research (BDR), 6-2-3 Furuedai, Suita, Osaka 565-0874, Japan

[2]Laboratory for Cell Polarity Regulation, RIKEN Center for Biosystems Dynamics Research (BDR), 6-2-3 Furuedai, Suita, Osaka 565-0874, Japan

[3]Department of Physics and Universal Biology Institute (UBI), Graduate School of Science, The University of Tokyo, 7-3-1 Hongo, Bunkyo-ku, Tokyo 113-0033, Japan

[4]Current address: Department of Biological Sciences, Graduate School of Science, The University of Tokyo, 2-11-16 Yayoi, Bunkyo-ku, Tokyo 113-0032, Japan

[5]Department of Macromolecular Science, Graduate School of Science, Osaka University, 1-1 Machikaneyama, Toyonaka, Osaka 565-0043, Japan

*These authors made equal contributions and are both available for correspondence

Running title: Structural analysis based on SHG microscopy

Corresponding authors:

Taro Ichimura, PhD

E-mail: tichimura@riken.jp

or

Tomonobu M. Watanabe, PhD

E-mail: tomowatanabe@riken.jp

Laboratory for Comprehensive Bioimaging,

RIKEN Center for Biosystems Dynamics Research,

6-2-3 Furuedai, Suita, Osaka 565-0874, Japan.

Tel.: 81-6-6155-0111

Fax: 81-6-6155-0112

This file includes

Supplementary Figures S1–S8.

SUPPLEMENTARY FIGURES

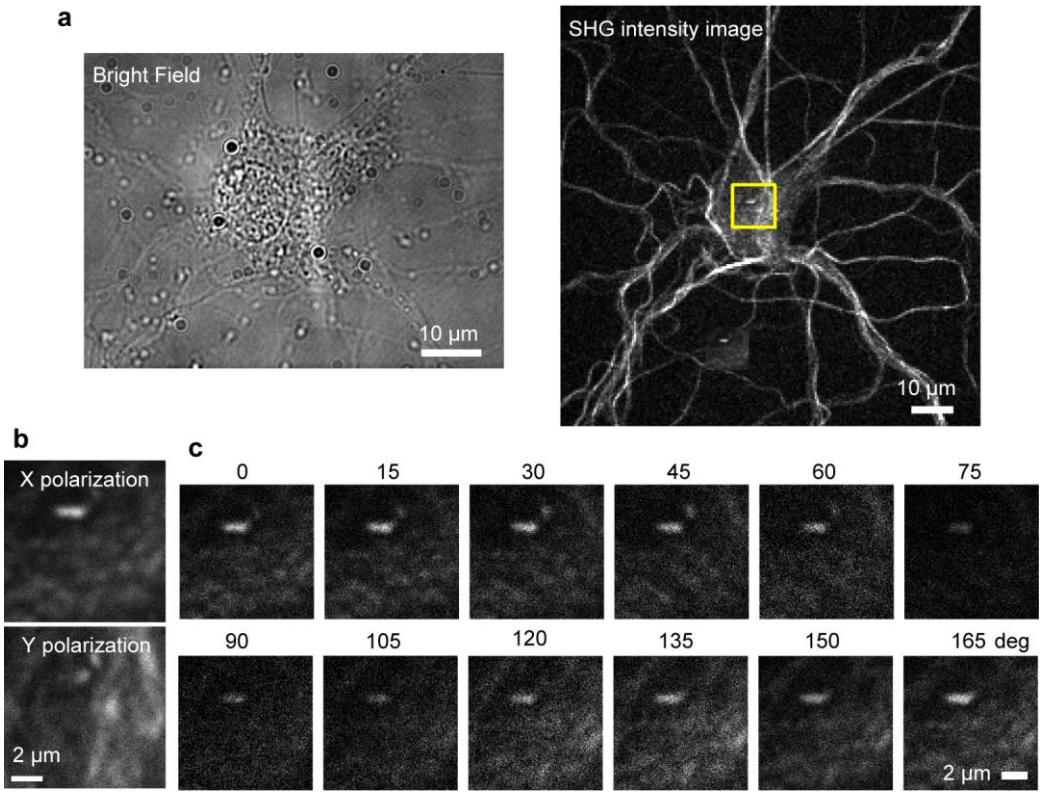

Figure S1. Typical images obtained by the present SHG microscope

(**a**) Transmission image (*left*) and SHG image (*right*) of a fixed nerve cell. (**b**) Enlarged image of *X*- (*upper*) and Y-polarization (*lower*) in the region indicated by the yellow rectangle in **a**. (**c**) Incident polarization dependence in *X*-polarization in SHG.

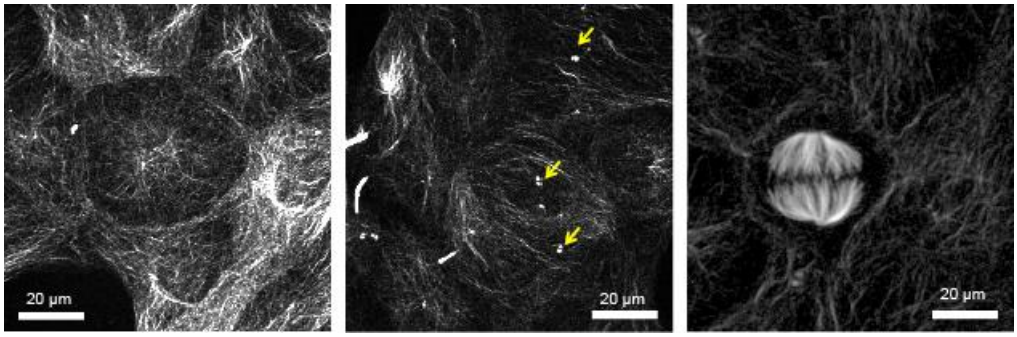

Figure S2. The SHG images of cells absorbed on high-purity SiO_2 glass

SHG images of MTs from epithelial cells fixed on high-purity SiO_2 glass in the interphase (*left* and *middle*), and during mitosis (*right*). Arrows in the left panel indicate individual pairs of centrioles.

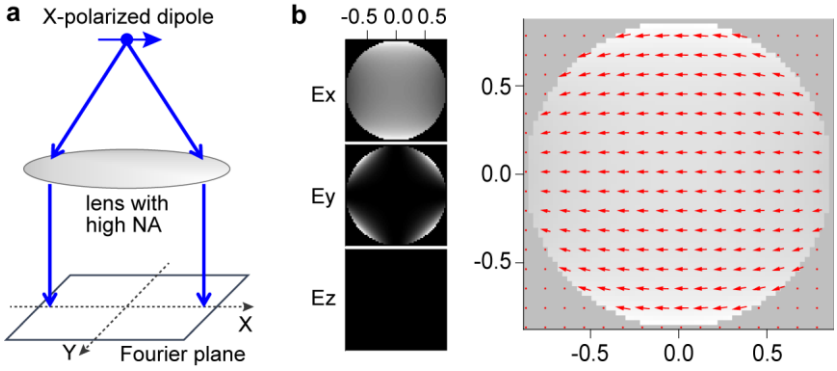

Figure S3. Theoretical calculation of the depolarization effect using an objective lens

(**a**) Schematic diagram of calculated system where optical radiation from a dipole at the SHG frequency is refracted by high NA lens and detected at the Fourier plane. Optical rays undergo depolarization when refracted at a high incident angle. (**b**) An example of depolarization caused by the lens. The dipole was linearly polarized in the *X*-direction. Intensity distribution of *X*-, *Y*-, and *Z*-polarized components (*left*), and total intensity distribution (*right*) of SHG light are shown with the polarization direction indicated by arrows.

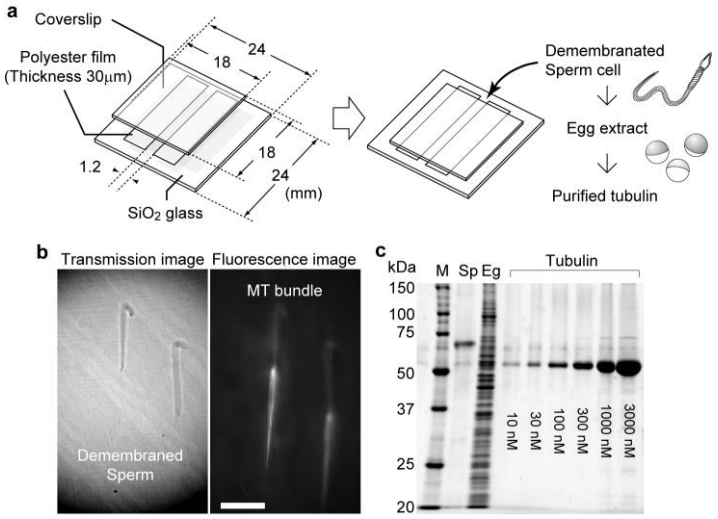

Figure S4. Sample preparation of MT bundles

(**a**) Schematic drawing of the flow chamber (*left*) and procedure to extend MT bundles from *Xenopus* sperm (*right*). (**b**) Transmission image (*left*) and fluorescent image (*right*) of the MT bundles labelled with Alexa 647. Scale bar, 20 μm. (**c**) SDS-PAGE of the proteins in the chamber after the observation. M, protein ladder marker; Sp, demembraned sperm; Eg, egg extracts, Tubulin, purified tubulin.

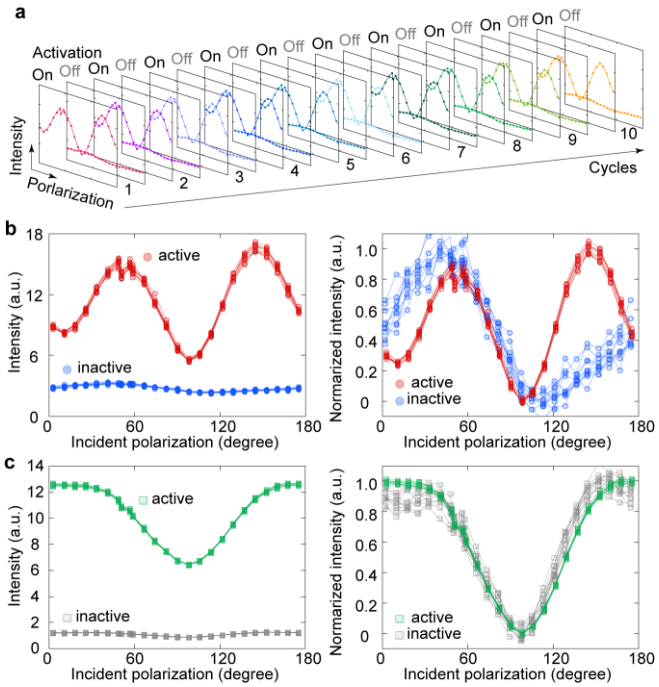

Figure S5. Time-lapse measurement of SHG and fluorescence in a Kohinoor crystal

(**a**) Repeated measurement of polarization dependence of SHG in a Kohinoor crystal between the active and inactive states. We obtained the fluorescence signal with the SHG measurement. (**b**) Typical 10 traces of the polarization dependence of SHG in the active state (*red*) and the inactive state (*blue*). The left panel shows raw data. In the right panel, the intensities were normalized from 0.0 to 1.0 to the minimum and maximum of the average of the 10 trials. (**c**) Typical 10 traces of the polarization dependence of fluorescence in the active state (*green*) and the inactive state (*grey*). The left panel shows raw data. In the right panel, the intensities were normalized from 0.0 to 1.0 to the minimum and maximum of the average of the 10 trials.

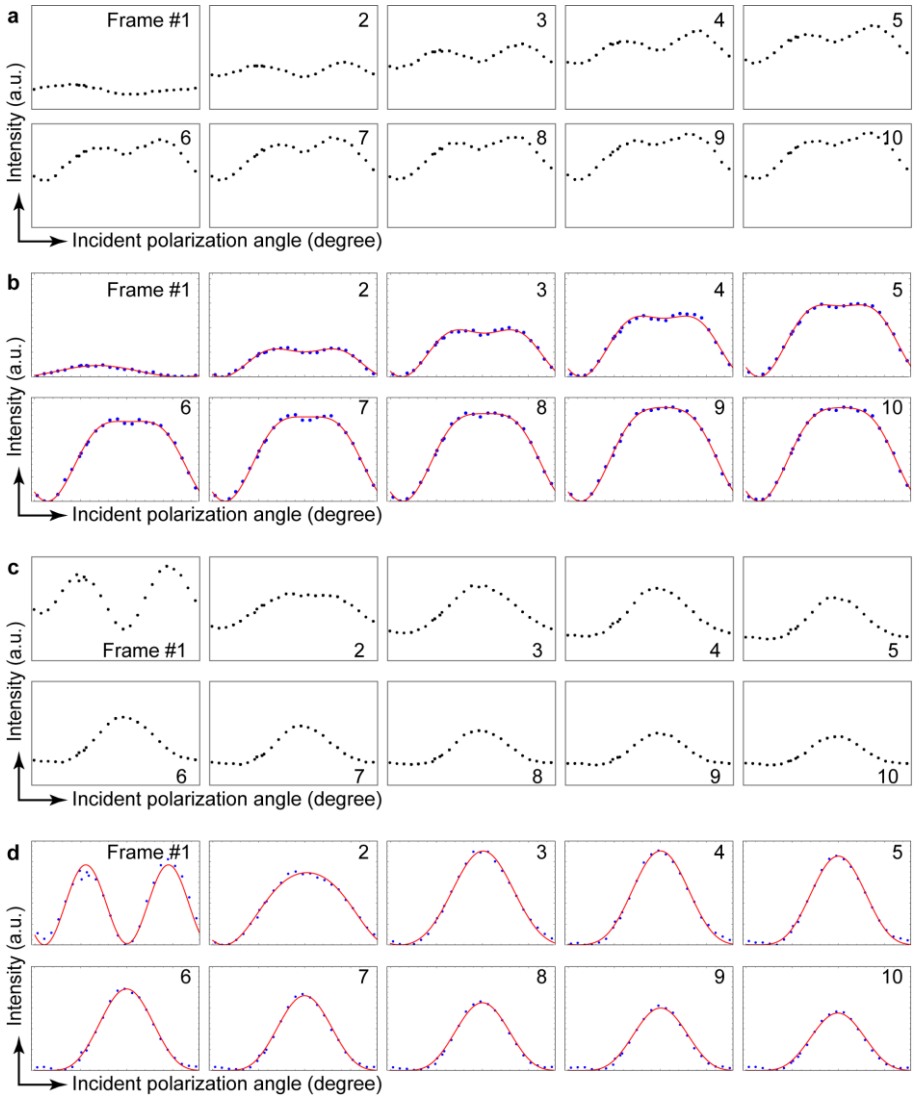

Figure S6. Phenomenological model fitting the SHG observation of the Kohinoor crystal

(**a**) Raw data for the time development of polarization dependence of SHG from a Kohinoor crystal during the transition from the inactive to the active state. (**b**) Traces in (**a**) after subtracting the effect of the fluorescent signal. Red lines are the fitted results. (**c**) Raw data of time development of polarization dependence of SHG from a Kohinoor crystal during the state transition from the active to the inactive state. (**d**) Traces of (**c**) after subtracting the effect of the fluorescent signal. Red lines are the fitted results. The constructed model and the fitting equation (Equation S6). The range of the incident polarization angle (horizontal axes) was 0° to 180° in all the panels.

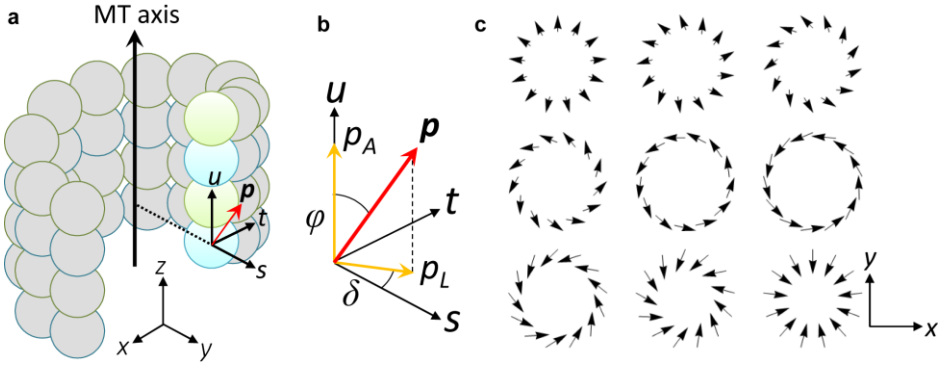

Figure S7. Schematics for explanation of validity of our estimation of the dipole angle in an MT

(**a**) Global coordinates defined in an MT (*x*,*y*,*z*) and local coordinates in a protofilament (s,*t*,*u*). (**b**) Orientation of dipole polarization, ***p***, in a tubulin subunit and its relationship with the local axes. (**c**) Possible alignments of lateral polarization components (p_L) in an MT projected in the *XY* plane.

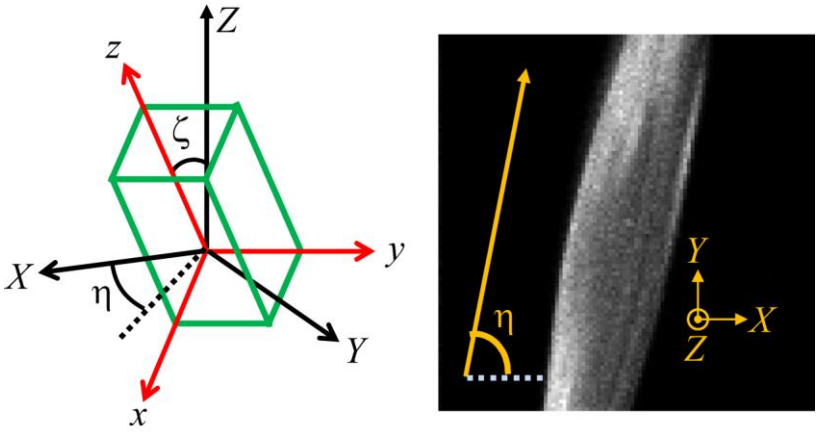

Figure S8. Schematic for phenomenological model of SHG observation in a Kohinoor crystal

Global coordinates (*x*,*y*,*z*) and laboratory coordinates (*X*,*Y*,*Z*) defined for Kohinoor crystal measurement (*left*). On the coverslip, the crystal was inclined by an angle of η from the laboratory axes of *X* (*right*).